REPORT DOCUMENTATION PAGE

Form Approved
OMB No. 0704-0188

1. REPORT DATE *(DD-MM-YYYY)*	2. REPORT TYPE	3. DATES COVERED *(From - To)*
	Technical Paper	

4. TITLE AND SUBTITLE

5a. CONTRACT NUMBER

5b. GRANT NUMBER

5c. PROGRAM ELEMENT NUMBER
62500F

6. AUTHOR(S)

5d. PROJECT NUMBER
2308

5e. TASK NUMBER
M4S7

5f. WORK UNIT NUMBER
345382

7. PERFORMING ORGANIZATION NAME(S) AND ADDRESS(ES)

8. PERFORMING ORGANIZATION REPORT

9. SPONSORING / MONITORING AGENCY NAME(S) AND ADDRESS(ES)

Air Force Research Laboratory (AFMC)
AFRL/PRS
5 Pollux Drive.
Edwards AFB CA 93524-7048

10. SPONSOR/MONITOR'S ACRONYM(S)

11. SPONSOR/MONITOR'S NUMBER(S)

12. DISTRIBUTION / AVAILABILITY STATEMENT

Approved for public release; distribution unlimited.

13. SUPPLEMENTARY NOTES

See attached 13 papers, all with the information on this page.

14. ABSTRACT

15. SUBJECT TERMS

16. SECURITY CLASSIFICATION OF:			17. LIMITATION OF ABSTRACT	18. NUMBER OF PAGES	19a. NAME OF RESPONSIBLE PERSON
a. REPORT	b. ABSTRACT	c. THIS PAGE			Kenette Gfeller
Unclassified	Unclassified	Unclassified	A		19b. TELEPHONE NUMBER *(include area code)* (661) 275-5016

AIAA-94-2464

Arcjet Diagnostics for Measuring Velocity, Density and Temperature

Ronald A. Spores, William A. Hargus Jr.
Phillips Laboratory
Edwards Air Force Base, California 93524

Jeffrey A. Pobst
Hughes STX Corporation
Phillips Laboratory
Edwards Air Force Base, California 93524

John H. Schilling, Frederick M. Lutfy,
and Daniel A. Erwin
University of Southern California
Department of Aerospace Engineering
Los Angeles, California 90089-1191

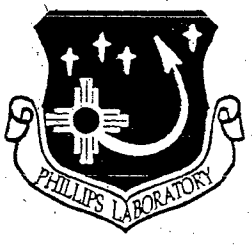

25th AIAA Plasmadynamics and Lasers Conference
June 20-23, 1994 / Colorado Springs, CO

Arcjet Diagnostics for Measuring Velocity, Density and Temperature

Ronald A. Spores*, William A. Hargus Jr.**
Phillips Laboratory, Edwards AFB, CA 93524

Jeffrey A. Pobst†
Hughes STX Corporation, Phillips Laboratory, Edwards AFB, CA 93524

John H. Schilling††, Frederick M. Lutfy††, Daniel A. Erwin‡
University of Southern California, Dept. of Aerospace Engineering, Los Angeles, CA 90089

Abstract

New diagnostic techniques to measure the fundamental plasma properties of an arcjet are being developed collaboratively between the Air Force Phillips Laboratory and the University of Southern California. These diagnostics are for measuring each of the principal parameters defining the plasma state within an arcjet: velocity, temperature, and density. Velocity measurements are being obtained from a new technique we have named Current Modulation Velocimetry (CMV). A current spike applied to the arcjet input current generates an optical emission event that is observed to travel downstream with the propellant flow. Observing this event at two axial locations, a fixed distance apart, provides an average bulk velocity of the gas flowing out of the arcjet nozzle. Species density measurements are to be obtained using Pulsed Electron Beam Fluorescence. A pulsed beam of focused electrons bombard a gas sample causing the resulting emitted fluorescence to be proportional to the local species density. Proper calibration with known samples can then provide absolute density values. Emission spectroscopy is employed to measure propellant excitation, rotational and vibrational temperatures inside the arcjet nozzle. Small (0.020") holes have been drilled through the arcjet nozzle to provide internal optical access. Velocity and density measurements are being conducted on the standard NASA Lewis 1kW arcjet while spectroscopic measurements are being taken on a 30kW class arcjet.

Introduction

Arcjets are expected to play an ever increasing role in satellite propulsion needs, primarily stationkeeping and on-orbit maneuvering in the near term. While the technology is considered viable enough to be deployed on a Telstar IV communications satellite for stationkeeping,[1] arcjets are far from a mature technology. After stationkeeping, one of the next steps for electric propulsion will be orbit transfer missions. With the upcoming ESEX flight test of a high power arcjet in late 1995[2], high power arcjet technology is being further advanced to fill this niche. However, in order to compete successfully with chemical propulsion systems for orbit transfer missions, further improvements in arcjet propulsion systems are still required.[3] If needed improvements in the performance level and efficiency of arcjets are to be achieved, an increased understanding of the fundamental physical processes that govern the operation of an arcjet is essential.

To increase the overall efficiency of an arcjet, it is important to understand the major energy losses, of which frozen flow is believed to be the dominant factor. Frozen flow losses of atomic species include: unrecovered dissociation, electronic excited states, and ionization, while molecular species also have rotational and vibrational energy states that are not fully converted to kinetic energy. The primary purpose of the temperature measurements described in this paper are to further investigate these energy loss mechanisms.

Another significant category of arcjet energy loss is velocity profile losses which are the result of thick internal boundary layers in the arcjet nozzle. These boundary layers are a direct result of the high propellant temperatures in the nozzle leading to high viscosity. To better understand profile losses, both gas velocity and density distributions must be known.

At present, only limited inroads have been made into the problem of plume density measurements, as standard diagnostic techniques like Laser Induced Fluorescence (LIF) cannot measure ground-state density, and techniques which can do so, such as XUV spectroscopy[4,5] are quite difficult to implement in practice. This paper discusses the calibration results for a new diagnostic technique which promises to provide point density measurements of any desired species in the plume.

For measuring velocity, Laser Induced Fluorescence has proven to be a very accurate and nonintrusive diagnostic technique. Unfortunately, it is rather expensive, it requires extensive expertise and it provides time-averaged values. We have developed a new velocity diagnostic that is inexpensive, fairly easy to operate, and is time-resolved. Velocity

* Research Scientist, Member AIAA
** Research Scientist, Student Member AIAA
† Scientist, Student Member AIAA
†† Research Assistant, Student Member AIAA
‡ Associate Professor, Member AIAA

fluctuations may also lead to viscous losses that can be recovered. Currently, there is no other time-resolved velocity measurement available that is applicable to arcjet plumes.

Information obtained from all three diagnostic techniques about the energy distribution in an arcjet is beneficial for both designing next-generation thrusters and for comparison with numerical models.

Part I: Time Resolved Measurements of 1 kW Arcjet Plumes using Current Modulation Velocimetry (CMV)

Background

Although much research, both experimental and numerical, has been conducted on arcjet plume characterization over the last 30 years, almost all previous studies assumed that the arcjet operates in a steady-state mode. However, when current is provided by a high frequency switching power supply, it is found that the current delivered to the arcjet modulates at the PPU switching frequency. How current modulation affects overall arcjet thruster performance is not fully understood. Current modulation is thought to potentially play a role in electrode erosion effects, while reference 6 clearly demonstrated that excited state frozen flow losses are affected by current modulation. It must still be resolved how current fluctuations affect mean velocity and frozen flow: dissociation, ionization vibrational and rotational energy losses.

In order to obtain velocity fluctuation data in an arcjet plume, it was necessary to develop a new velocity diagnostic.[7] This diagnostic, called current modulation velocimetry (CMV), measures instantaneous velocity over a spatial region between two points. A current spike applied to the arcjet input current generated an optical event that was observed to travel downstream with the gas flow. Observing this event at two locations a fixed distance apart implies an average bulk velocity of the gas flowing out of the arcjet nozzle. CMV is the only technique presently being employed that provides instantaneous velocity measurements of the arcjet plasma with temporal resolution of a few microseconds. The disadvantage of the CMV technique is that it employs spatial averaging over an axial distance of several mm and it is a line-of-sight radially integrated technique.

In Reference 7, the CMV technique was used to measure fluctuations in velocity as large as ±20% of the mean velocity (see Figure 1). The source of the fluctuations in the gas velocity was not ascertained, though it was surmised that the velocity fluctuations might be linked to the ripple in the current applied to the arcjet.

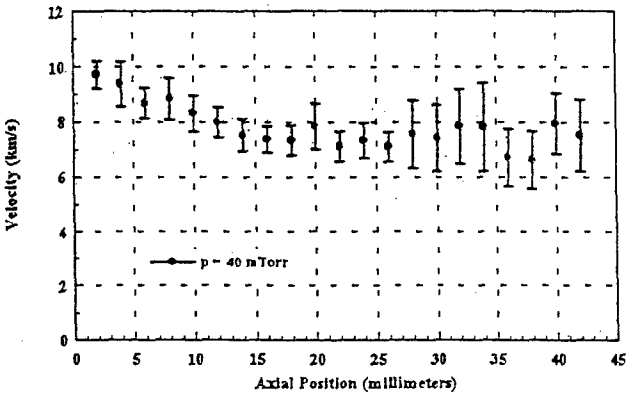

Figure 1: Mean Velocities and Fluctuations Downstream of Arcjet Nozzle Exit

This work employs the use of an automated triggering circuit in conjunction with the CMV technique to measure velocity at a time when the current ripple is at a specified level. This allows multiple velocity measurements taken for statistical purposes to be triggered at the same phase in the current ripple.

Experimental Description

Experimental Conditions and Equipment

CMV experiments were conducted in the Optical Diagnostics Chamber (see Figure 2) of the Air Force Phillips Laboratory Electric Propulsion Lab. The arcjet used here is a 1-kW-class radiatively-cooled engine, constructed and furnished by NASA Lewis Research Center. Standard operating conditions of 1.13kW (112.5 V and 10.1 A), with 13.7 mg/s mass flow of hydrogen propellant were employed. The experiments were conducted with a background chamber pressure of ~35 millitorr.

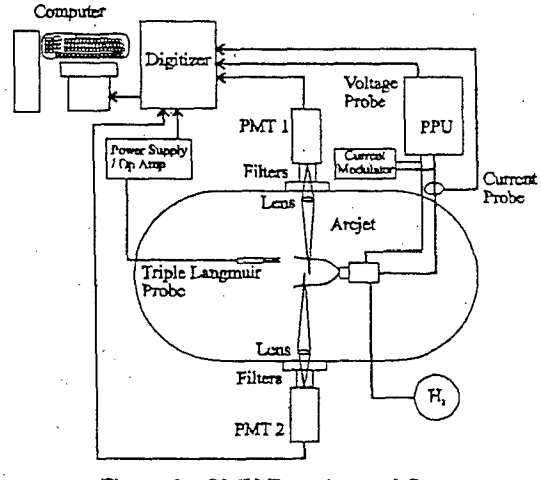

Figure 2: CMV Experimental Setup

The operating conditions are similar to those of other groups involved in optical diagnostic velocity measurements,[8] allowing comparison of experimental results to be made.

Power was provided by a NASA Lewis 1-kW power processing unit (PPU). The PPU is a high-frequency switching power supply, operating at 16 kHz, and generates a 20% peak-to-peak current ripple. The vacuum system consists of an aluminum chamber, 3 m in length and 2 m in diameter. Two 9500-cfm Roots blowers evacuate the chamber; each is backed by a 1600-cfm blower and a mechanical pump

For the optical emission measurements, two Hamamatsu R943-02 photomultiplier tubes (PMT) were used. A 10 nm Melles Griot interference filter (λ_0=656.3 nm) and appropriate neutral density filters were placed in front of each PMT to insure that only the Hα emission was observed. The optics train of each detection system is identical. All optical, current and voltage signals were recorded on a Tektronix DSA 601 digital signal analyzer or a Tektronix TDS 644A digital oscilloscope.

Current Modulation Velocimetry

The current spike needed for CMV is generated by a simple RC shunt circuit which is installed in parallel with the arcjet. Upon closing a switch between this circuit and the arcjet circuit, the arcjet voltage appears across the shunt, charging the capacitor over several 1-microsecond RC time constants. The shunt current is thus a several-ampere pulse lasting a few microseconds. The shunt current is subtracted from the arcjet current, which results in a spiked current dropout (the total current from the PPU is constant during this time, as it is held up by an output inductor of several mH).

The positive ring of the current pulse generates a sharp emission spike. The emission spike is delayed with respect to the current spike; this delay is equal to the integral of $1/v$ over the distance from the arc-heating region to the detection station, where v is the plume velocity as a function of axial position. A portion of the flow inside the arcjet is thus "tagged" by the current pulse.

The emission spike is recorded at two different downstream locations. A best-fit transformation between the two digitized emission spikes is determined using the standard Levenberg-Marquardt method.[10] The generated covariance matrix gives a measure of the confidence interval of the best-fit parameters, assuming the measurement of the optical signal to be subject to uniform, normally-distributed scatter. Error bars indicate the precision of each measured velocity and are computed using a one-standard-deviation confidence interval of the horizontal translation (the time delay between the two emission spikes).

The current and emission spikes are of a few microseconds duration. Time delays between the emission spikes at the two locations can be resolved to within one nanosecond, leading to a velocity measurement whose accuracy is in the range 30–60 m/s for plume velocities on the order 5–10 km/s; this accuracy is comparable to those of recent CW-LIF results.[8,9]

Note that the velocity measurements obtained with CMV, while still position-averaged over the detector separation (here, 3.29±0.05 mm), are instantaneous. The principal velocity diagnostic presently being used for arcjets is continuous wave (CW) laser induced fluorescence (LIF)[8,9] which provides spatially resolved mean velocity measurements but with very limited temporal resolution. LIF measurements, determine the absorption lineshape by scanning in laser wavelength, which takes a minimum of several seconds to determine a velocity. In principle, a Doppler-shifted emission lineshape could be recorded instantaneously by a spectrograph and a gated imaging detector, but we know of no plume measurements in which Doppler shifts have been so measured. (In the recent Stuttgart work of Zube and Auweter-Kurtz,[11] instantaneous lineshapes were recorded in order to measure arc properties [gas excitation temperature and electron density].)

An automatic optio-isolated MOSFET circuit allowed computer control of the start time and duration of the modulation to the arcjet current (see Figure 3). The switch closes based upon a trigger from a pulse generator. The generator issues a pulse when the measured circuit current reaches a pre-set trigger level and after a computer request for an event has been received. This allows the operator to issue a request for a measurement and have that measurement take place the next time the PPU current ripple is at the specified phase of the current ripple.

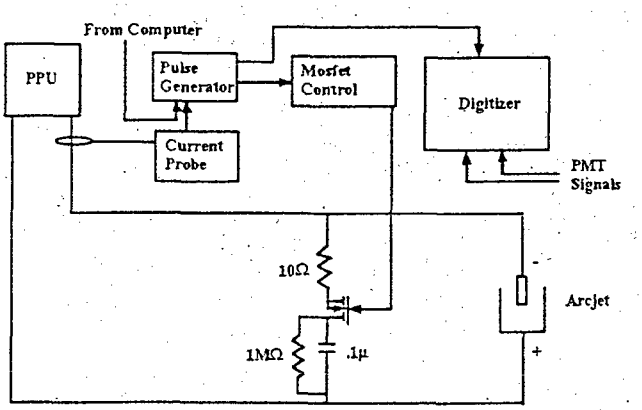

Figure 3: Automated CMV Setup

Results

Examining the CMV Technique

Figure 4 illustrates the effect of the CMV technique on the arcjet's current and voltage. The arcjet current ripple (caused by the switching nature of the arcjet PPU) is briefly interrupted by a sudden loss while the capacitor charges. The

current then rings upward and significantly overshoots its previous maximum. After quickly dampening, the current begins its previous PPU - induced ripple. Note that the voltage across the arcjet also has a characteristic ripple and that it is almost 180° out of phase of the current. This is expected due to the negative impedance characteristic found in arcjet devices.[12]

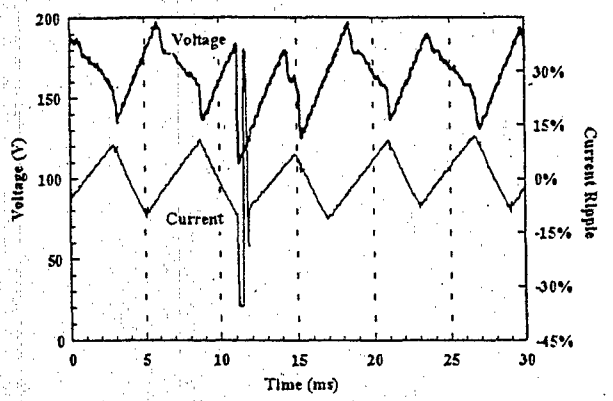

Figure 4: Typical CMV Effect on Arcjet Current and Voltage

This figure reveals an unexpected behavior of the arcjet voltage which occurs as current is redirected into the capacitor of the RC circuit. The voltage drops suddenly as the current drops and then gradually ramps upward to previous levels without ringing. It then begins it's periodic ripple.

Figure 5 looks at the current and voltage on a more resolved timescale. The voltage and current both drop quickly after the CMV gate pulse closes the circuit and then simultaneously change in slope. The voltage begins to ramp back upward to previous levels, while the current decreases in a more gradual way then before. At t = 11.5 microseconds, the current then shoots upward with no apparent reaction by the arcjet voltage. It then returns to previous levels with some minimal ringing.

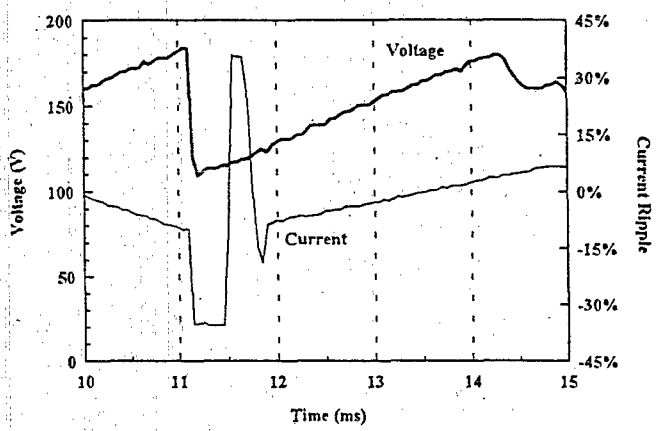

Figure 5: Typical CMV Effect, Resolved View

In addition to arcjet current and voltage probes, a Hall-effect current probe was placed on the RC circuit. Two digitizing oscilloscopes were used in order to simultaneously observe several transient signals. These include: the arcjet current and voltage, the current through the circuit when the switch is closed, the gate controlling the switch, and the two emission traces taken from the photomultiplier tubes. The resulting scope traces are shown together with arbitrary vertical units in Figure 6.

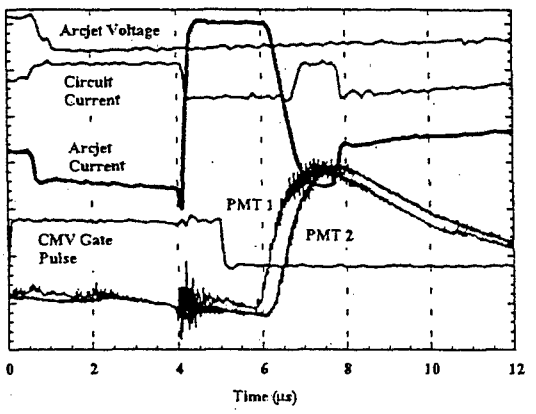

Figure 6: Arcjet and CMV Properties vs. Time

The current measured through the circuit is inversely proportional to the current going to the arcjet, as expected. When the circuit current drops below its initial level (no current through the circuit), it indicates that current through the circuit has reversed direction and that the capacitor is discharging; this is an expected reason for the arcjet current to overshoot. The rapid decrease in arcjet current drops below its initial level and a short ring in circuit current is momentarily seen. This is followed by a slow rise back up to zero in circuit current and a return to previous ripple behavior in arc current.

As noted earlier, the arcjet voltage follows the current when the CMV gate is closed and decreases in value rapidly. As current begins to flow through the circuit, however, the arcjet voltage begins a slow rise back to its previous level, seemingly unaffected by other changes in arcjet current.

All optical events are observed downstream of the arcjet nozzle exit plane. One photomultiplier tube (with a Hydrogen Balmer-alpha notch filter) is focused to a small control volume of diameter 1 mm from the nozzle exit centerline, while a second identical PMT system is focused to a control volume located 3.29 mm downstream of the nozzle exit. Noise in the optical emission , which starts at 4 µsec in Figure 6, (it has been verified to be completely optical in nature) is seen simultaneously by both PMT's when the arcjet current first begins to rise. This is then followed by a much more significant increase in Balmer-alpha emission at 6 µsec. This increase occurs at both control volumes but at different times, being seen first at the upstream PMT focal point.

The optical noise seen as the arcjet current first rises does not demonstrate a time shift as does the emission that follows it. Thus, the two different emission phenomena seen at 4 and 6 μsec are most likely caused by different excitation processes.

It was previously stated[7] that the optical emission phenomenon that progresses downstream in the plume comes from electron recombination which repopulates the uppermost energy levels. The electrons subsequently cascade downward to repopulate the H Balmer excited states which are then observed by the PMTs. This explanation still appears valid for the large time dependent emission peaks which begin at 6 μsec. However, the optical noise seen at 4 μsec must warrant a separate explanation due to its time independent nature. One likely theory is that the optical emission at 4 μsec in the arcjet plume is caused by the reabsorption of photons generated at the arc core inside the constrictor region of the arcjet as suggested by Cohen, et. al.[13]

When starting the arcjet, the voltage characteristic of the thruster changes slowly as the nozzle heats up. The mean voltage increases while the heating takes place. Prior to reaching a steady state voltage a curious behavior is noted to intermittently take place when implementing the CMV technique. Though the proper trigger gate and initial current behavior remain the same, differences in the current overshoot appear to lead to a situation where the emission spikes used for velocimetry do not appear. This situation is shown in Figure 7.

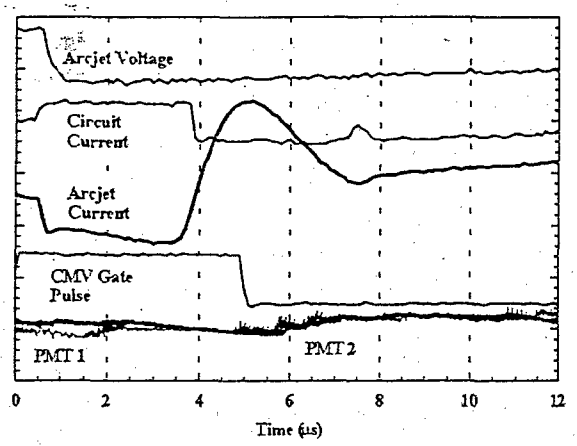

Figure 7: Arcjet and CMV Properties vs. Time
No CMV Emission

Note that the first four microseconds of the "non-emission" case are essentially identical to the previous case depicted in Figure 6 where Balmer-alpha emission is present. The sharp rise in current that followed in the previous case is not present and both types of emission previously observed are absent. This prevents a CMV velocity measurement from being made and appears only in situations where the arcjet voltage is lower than the standard operating condition of 112.5V and 10.1A. As the arcjet is operated at lower current (and consequently higher voltage) this behavior is no longer seen. Therefore, the implementation of the CMV technique appears to rely upon a minimum voltage across the arcjet in order to generate a subsequent ringing in the arcjet current when current is redirected into an RC circuit. It is likely that this subsequent ringing is the key phenomena, inducing the emission which proceeds downstream, and thus allowing time-of-flight velocity measurements to be made.

Velocity Measurements

In order to make velocity measurements while "linked" to the PPU current ripple, a computer controlled MOSFET gate switch was implemented. In using this switch a new parameter in CMV operation was required, this being the length of time that the RC circuit was closed (the gate width) and in parallel with the arcjet. Variation of the gate width took place and results of interest are shown in Figure 8.

The gate width was varied from ½ μs to 100's of μs in length. The mean velocity measured was basically the same as long as the gate width was above 3 μs. Mean velocities measured were observed to decrease as the pulse width was decreased for the equivalent test conditions. Figure 8 demonstrates this behavior for three different power conditions. The $\frac{P}{\dot{m}}$ was held constant by reducing the mass flow through the arcjet as power was decreased. Note that for the 1.13kW case, the decrease in velocity measured was less evident than in the lower power cases.

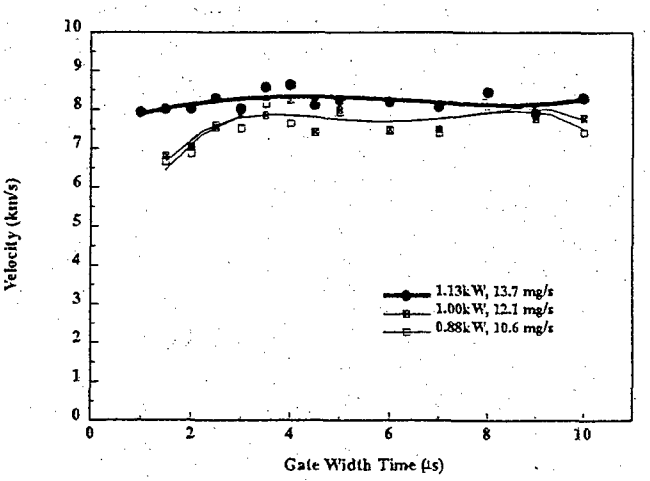

Figure 8: Mean Exit Plane Velocity Measurements vs. CMV gate Width

The shorter gate widths cause a change in "measured" velocity between the two emission collection points in the plume. When the RC circuit is connected to the arcjet for less than 3 microseconds, the behavior of current and voltage is similar to that seen in Figure 7 where the voltage is insufficient for CMV emission to take place. The short-gate-width-behavior differs from that of Figure 7 since CMV emission occurs, though at lower intensities than desirable.

These lower velocity measurements are not due to a lower signal intensity but are suspect in the fact that the emission shape is less defined. It is possible that the recombination processes that repopulate the uppermost electronic levels are incomplete when the circuit is in parallel with the arcjet for short durations. We surmise that the lower velocities result from utilizing a waveform that undergoes change as it traverses between the two imaging control volumes.

The average velocity and standard deviation of velocity fluctuation measured at the nozzle exit using CMV with a gate width larger than 3 microseconds is shown in Figure 9 along with LIF longitudinal velocity data from Liebeskind et al.[14]

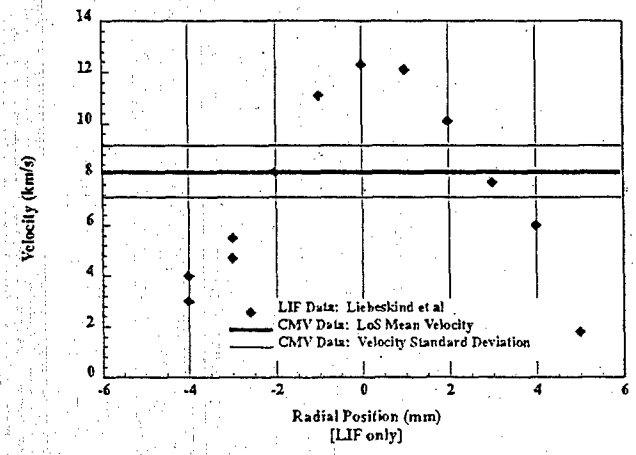

Figure 9: CMV and LIF 1kW Arcjet Velocities at Nozzle Exit

In this figure, radial, point-specific, time-averaged LIF velocity measurements are compared with a mean, line-of-sight CMV velocity shown as a line across the graph with two dashed lines representing the standard deviation of observed velocity fluctuations. Though the density of excited state H is not available to weigh the LIF data and obtain an mean LIF velocity, relatively good agreement between these two techniques is observed.

It has previously been surmised that the fluctuations shown in Figure 9 and in our previous work[7] have been a consequence of the oscillating nature of the internal energy dissipation of a 1kW arcjet due to the PPU current modulations. Triggering at a constant PPU ripple level, Figure 10 shows measured mean velocity and standard deviations while triggering at constant current ripple phase.

In Figure 10, no change in mean velocity value or substantive change in fluctuations can be directly related to PPU phase angle. If the velocity is changing with respect to the current ripple, a significant decrease in fluctuation and change in mean velocity should be observed.

With no apparent connection between the PPU ripple and the mean velocity, the question arises once again: What is causing the fluctuations in arcjet plume velocity? Attempts at determining a fluctuation frequency through a real time transformation of the difference between the emission from the two imaging points provide inconclusive results. Certainly finding a fundamental frequency of velocity fluctuation might narrow the possible causes of this phenomenon, though it remains to be seen if a single cause can be pinpointed.

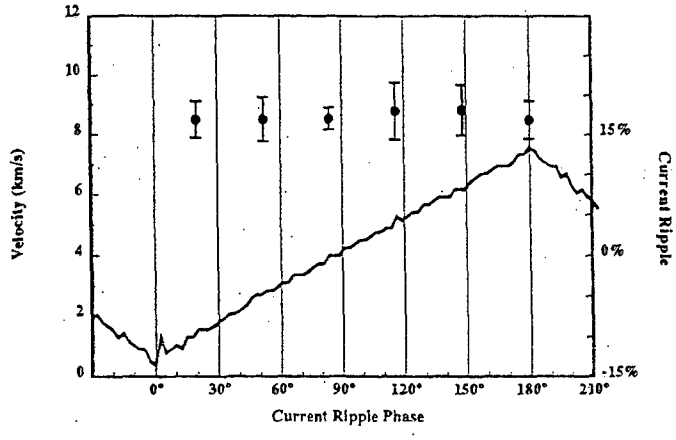

Figure 10: CMV Velocity Exit Plane Measurements at Various Current Ripple Phases

Part II: Pulsed Electron Beam Fluorescence

Background

This section discusses a new diagnostic which uses pulsed electron beam fluorescence (PEBF) to measure total species density in the plume. Since electron collisions are capable of exciting any atom, molecule, or ion in any state, an electron beam fluorescence technique can measure the density of a species independent of state. We expect that the use of PEBF will produce accurate species-specific ground state density measurements in arcjet plumes, with spatial resolution of approximately one millimeter.

The electron beam fluorescence technique has been used in extremely low-density flows for almost thirty years.[17,18] Traditionally, low-current dc electron beams are used to excite atoms and molecules in the flow and the resulting fluorescent emission is collected and analyzed. At densities of greater than 10^{16} cm,$^{-3}$ collisional quenching causes the signal to lose density dependence. Moreover, beam divergence causes a significant loss of spatial resolution at such densities. This precludes the use of conventional EBF in an arcjet plume.

However, by using a high-current, pulsed electron beam in conjunction with a fast gated detector it is possible to use electron beam fluorescence at much higher densities. Quenching will still cause the emitted signal to take on a Stern-Vollmer form, with time-integrated emission sublinearly dependent on density. However, if the pulse length is small compared to the quenching timescale, the peak emission will be unaffected by quenching and will retain full density dependence. Also, at high currents and moderate to high gas pressures, an electrostatic self-focussing effect has been observed which maintains beam collimation despite scattering effects.[19]

Until recently, it was not practical to generate pulsed electron beams of sufficient energy or current for diagnostic use. However, the recent development of pseudospark discharge switches has provided a simple and compact means of generating electron beams with the necessary characteristics. We have explored the use of such devices for diagnostic purposes for several years,[19] and are currently developing a facility for applying PEBF diagnostics to low-power arcjet plumes.

PEBF Operation

To simplify interpretation of the initial PEBF results, we have chosen to use helium as the arcjet propellant. Helium is a monoatomic gas and thus we simplify the number of possible excitation modes. As discussed in reference 15, this diagnostic is expected to also be applicable to polyatomic species, however, fluorescence signal interpretation will be more involved. The plume of a low-power helium arcjet consists primarily of ground-state helium atoms at a density of order $\sim 10^{16}$ cm,$^{-3}$ with a small population of excited-state atoms, ions, and free electrons. When an electron beam passes through the plume, it will excite atoms and ions by inelastic collisions regardless of initial state.

The population of atoms excited to state i by a pulsed beam is given by the following equation:

$$N_i = I_b T_b L N_o Q_{oi} \qquad (1)$$

where I_b and T_b are beam current and duration, L is probe volume length, N_o is ground state number density and Q_{oi} is the cross section for electron impact ionization to state i.

For ground-state helium excited to the N=3 state by 30 kV electrons, this cross section[20] is 4.2×10^{-19}cm.^{2} Assuming a beam current of 100A and 10ns duration, a probe volume of 1mm^3, and a local density of 10^{16} cm^{-3}, we expect a population of 2.6×10^9 N=3 atoms in the probe volume. For comparison, with a local temperature of 10,000K and electron density of 10^{14} the Saha equation[21] gives a much lower background N=3 population of 1.3×10^7 cm^{-3}.

The cross-section for collisional quenching of the N=3 state in helium[22] is approximately 1.5×10^{-15}cm.^{2} The quenching rate is given by:

$$D_{io} = 2 N_o Q_{io} \{2kT/pM_g\}^{1/2} \qquad (2)$$

At the temperature and density expected in the plume, this corresponds to a quenching timescale of 300ns, much longer than the pulse length or the signal collection time. Therefore, the time-dependent signal will be directly proportional to the local number density. Given the spontaneous emission coefficients A_{31} and A_{32} for helium (5.66×10^8 and 0.13×10^8, respectively[23]), the anticipated signal for a local density of 10^{16} cm^{-3} is 6.0×10^8 photons at 5015.7Å emitted during the ten nanoseconds immediately following excitation.

The magnitude of this signal, along with its linear density dependence, is the primary motivation behind the PEBF technique. Since the signal is several orders of magnitude greater than the background emission of the plume, it is easy to detect and isolate. After calibration of the experiment with a static gas of known density, it is straightforward to extract the number density in the probe volume. Furthermore, this signal is strong enough to be easily detectable even if densities are an order of magnitude less than expected, and fast enough to overcome quenching at densities an order of magnitude larger than expected.

Successful use of the PEBF technique hinges on the ability to generate a pulsed electron beam with appropriate current, energy, pulse length, and diameter. As pseudospark discharge

devices are capable of producing beams with electron energies of 20-50kV, currents of several hundred amps, pulse lengths of order 10ns, and beam diameters of about 1mm.[15,24,25] The electron gun is sensitive to the environment in the discharge chamber, thus, a separate gas feed is required in addition to a vacuum isolation system between the gun and the test chamber.

The utility of electron-beam fluorescence would be seriously limited by beam divergence were it not for the fortuitous occurrence of a self-focussing effect.[17] If a high-current beam passes through a relatively high-density gas flow, it will produce a significant degree of ionization. The positive ions will not move noticeably during a 10-ns pulse, but even 1eV secondary electrons will move several millimeters during this period, and therefore leave the beam path. This results in a narrow core of positive charge surrounded by a negative sheath, and tends to confine the electron beam.

If the positive ion density in the beam path is comparable to the electron density in the beam, this self-focussing will largely prevent beam divergence due to space-charge repulsion. Calculations based on known ionization and scattering cross-sections indicate that self-focussing should occur at densities between 10^{15} cm^{-3} and 10^{17} cm^{-3}, and possibly higher[15], which is consistent with our observations. This density range covers the expected plume environment, so beam divergence should not be a factor in this application.

Experimental Apparatus

Initial PEBF measurements will be made on a NASA Lewis-designed 1-kW helium arcjet. The use of helium simplifies the calibration procedure significantly as opposed to performing calibration with hydrogen. The arcjet is installed in a steel chamber of 1-meter diameter, with a 6000cfm vacuum system to maintain background pressure within acceptable limits during operation.

While the arcjet facility is under construction, we have begun calibration of the PEBF system in a smaller test facility. A schematic of the calibration facility is shown in Figure 11. The pulsed electron gun (PEG), which operates at 35kV on hydrogen, fires into a chamber containing the test gas (helium or nitrogen). The subsequent fluorescence trace is captured using a Hamamatsu R943-02 photomultiplier tube through a double .85m Spex spectrometer. The light from a small control volume in the calibration chamber is focused through a lens and mirror combination to the spectrometer entrance slit.

Calibration Experiment

Calibration was conducted by filling the chamber with helium and nitrogen gas to known pressures from zero to 200 microns, firing the gun, and measuring the fluorescence signal at the desired wavelength. Unfortunately, it is not possible to calibrate at pressures higher than 200 microns in this facility due to interference with gun operation from contamination of the discharge chamber with the test gas.

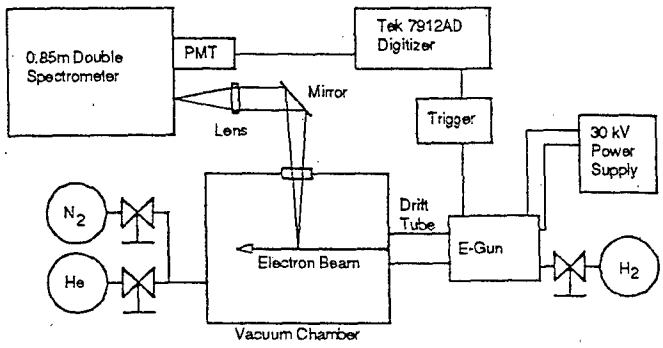

Figure 11: Calibration Facility Schematic

The gun was fired thirty-two times for each condition, and the results averaged by the digitizer to produce a representative signal vs. time trace. The peak and time-integrated signals were compared with the known pressure to determine the calibration curve. Signal averaging was used to minimize the effect of pulse-to-pulse variations in beam current and collimation.

In operational use, a Rogowski coil will be used to measure beam current, and the observed fluorescence will be correlated with the current to reduce the effects of beam variations, and possibly compensate for trigger jitter as well. Unfortunately, commercially available coils do not operate well in the interference environment created by the electron beam. While we have manufactured shielded Rogowski coils for this purpose, they could not be easily mounted in the calibration facility.

Calibration Results

The photomultiplier tube (PMT) output from the calibration experiments was recorded versus time at varying test gas pressures. These plots are displayed in Figures 12 and 13. As expected, the peak value of the observed signal increases with rising species density, and Figure 14 illustrates the nearly linear relationship between density and integrated signal strength for helium emission. The relationship between integrated signal strength and nitrogen emission is not as linear.

The FWHM of the curves and their associated delay times decrease with increasing gas pressure. One possible explanation for this phenomenon is that the interface between the gun chamber and test section is restricted by a 3mm diameter orifice. Since the gun operates on hydrogen, it is necessary to maintain the H_2 pressure inside the gun chamber

at a higher value than the test chamber to minimize possible contamination. However, as the pressure differential between chambers increases, there is a corresponding rise in H_2 flow rate from the PEG to the test section. The dynamics associated with higher Hydrogen flow rates inside the PEG may cause instabilities in the discharge.

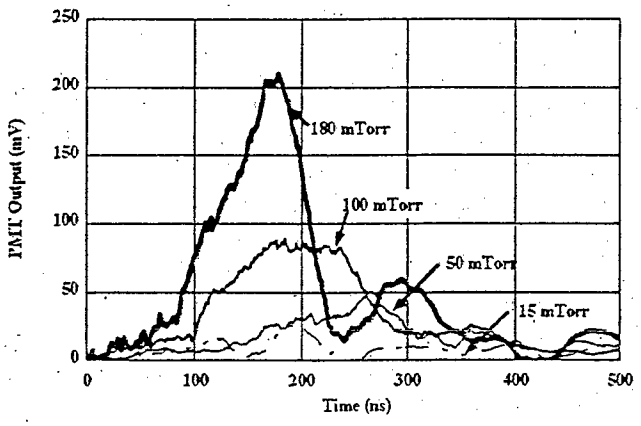

Figure 12: Signal vs. Time, Helium Gas

Some work remains to verify these results. To investigate facility-dependent effects, the calibration must be repeated in the arcjet test chamber before operational use. Furthermore, it is desirable to conduct the calibration with beam-current measuring equipment in place and with an appropriate vacuum isolation system. Although the averaged-signal method discussed here should compensate for pulse-to-pulse irregularities in beam current, collimation, and trigger time, the possibility of spurious results due to an interaction between the chamber and gun environments cannot be ruled out.

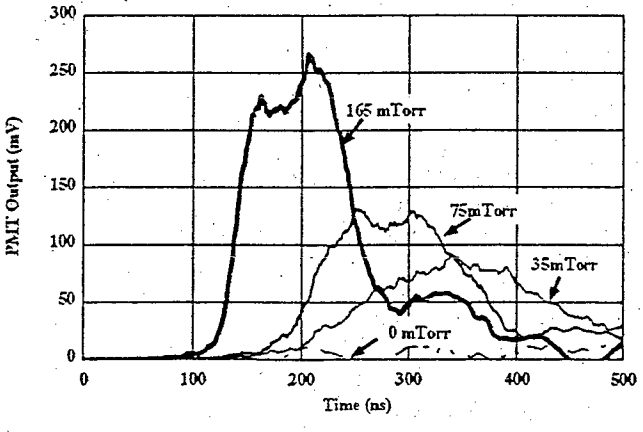

Figure 13: Signal vs. time, Nitrogen Gas

Nonetheless, the results reported here indicate that the PEBF system can be used as an accurate density diagnostic in an arcjet plume environment. The linear relationship between helium density and peak signal will significantly simplify analysis, assuming that the peak signal can be captured using a gated detector. Following a final calibration in the arcjet test chamber, and assuming similar results to those already observed, measurements of arcjet plume density using the PEBF technique will begin shortly.

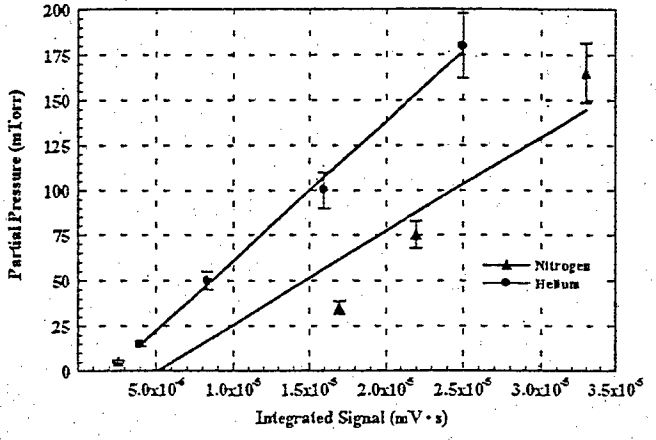

Figure 14: Integrated Signal vs. Pressure, He and N_2

Part III: Energy Deposition Modes within the Nozzle of a High Power Ammonia Arcjet

Background

Greater understanding of the arcjet internal chemical kinetics is required to improve high power arcjet performance. While extensive work has been performed in the plume region, the investigation must shift to the interior to better understand the plasma expansion process. Therefore, a research effort was initiated to determine the characteristics of electric arc energy deposition to propellant flow within the nozzle of the arcjet using emission spectroscopy. To gain access to the plasma inside the arcjet nozzle interior, three optical access ports were equally spaced axially along the expansion nozzle of a 26 kW class NH_3 arcjet. The results obtained will be used to design new, more efficient nozzles for 30 kW class arcjets and to increase the data base for improved computational codes. Neutral excitation, ionic excitation, vibrational, and rotational temperatures were determined using a variety of spectroscopic techniques.

Experimental Technique

Experimental Setup

The arcjet used for this research program was the USAF 26 kW class laboratory thruster. The basic arcjet configuration and design is extensively discussed in reference 26. The area ratio of the nozzle is 100 with a constrictor length and

diameter of 0.1 inches, an expansion angle of 38°, and a nozzle length of 1.307 inches. The arcjet was operated on 250 mg/sec of ammonia at a power level of 17.7 kW (151 A, 117 V)[26] in a 200 millitorr background environment.

Much of the work discussed here parallels that of Zube and Myers with the exception that they worked exclusively on low power arcjets while this effort pertains only to the 30 kW class arcjet.[27] Note that the three optical access holes were drilled through both sides of the nozzle, as shown in Figure 15, to minimize internal reflections. Zube and Autweter-Kurtz[11] likewise used access holes completely through the arcjet in their study of the constrictor region and showed that reflections were insignificant when compared to the total signal. From the interior wall of the arcjet nozzle, a 0.020 inch diameter optical access passage was generated for the first 0.100 inches; at that point the port was expanded to 0.080 inches to the outer edge of the anode/nozzle. The most upstream optical access port was placed just downstream of the constrictor (0.100 inches) while the remaining two optical ports were positioned equidistantly between the first port and the nozzle exit. The ratios of the optical access port areas to the corresponding expansion nozzle area compared favorably with those of Zube and Myers.[27] They determined that the optical access ports did not affect the performance of the arcjet within the resolution of their thrust stand (<2%). A comparison of thrust measurements, both with the holes open and then plugged, is the best method for determining whether the optical access technique is intrusive. Unfortunately, thrust stand measurements have not been taken as of this writing. It is still believed that whereas the area ratios of the holes to access point nozzle areas are comparable or smaller than those of Zube and Myers, it is reasonable to assume that these access ports do not perturb the arcjet operating characteristics significantly. Further, no preferential arc attachment was seen near or around the optical access ports and no other non-standard arc behavior was in evidence throughout testing.

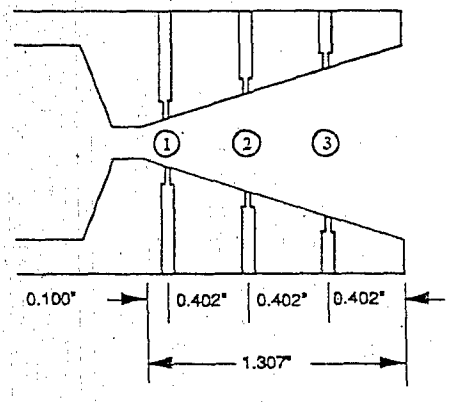

Figure 15: Optical Access holes in Arcjet Nozzle. Hole Numbers are referred to throughout this section.

This project was conducted in vacuum chamber 2 of the USAF Electric Propulsion Laboratory of the Phillips Laboratory at Edwards AFB, California. An emission spectroscopy system was developed specifically for internal arcjet optical diagnostics.[26] Figure 16 shows the optical train used to collect the emission signal from the arcjet interior through the optical access ports. After the signal is collected, it is focused onto the entrance slit of a Czerny-Turner 0.5 m Acton Research SpectraPro-500 spectrometer. The spectrometer contained a turret with three holographically blazed gratings of 2400, 1200, and 600 groove/mm. At a wavelength of 435.8 and with a 1200 groove/mm grating, the system had a resolution of 0.05 nm in the first order. A Princeton Instruments thermo-electrically cooled CCD detector with a UV scintillator was used to obtain the resultant spectra. A relative intensity calibration of the spectroscopy system was performed by focusing on the filament of a quartz tungsten ribbon lamp with a calibration traceable to the National Institute of Standards and Technology. The arcjet was placed on a three axis translation system with repeatability of 0.001 inches and a straight line accuracy of 0.0005 in/in to provide proper alignment of the spectroscopy collection system with the optical access holes.

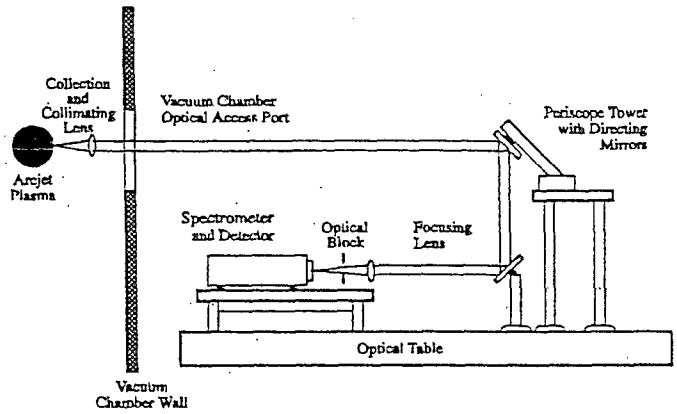

Figure 16: Emission Spectroscopy Experimental Setup

Spectroscopic Techniques

For the experiments discussed here, the standard Boltzmann plot technique was employed to obtain excited state temperatures. If the spectral resolution allowed, data from 5-10 transition lines were used with the following equation:

$$\ln\left[\frac{I_{ij}\lambda_{ij}}{cA_{ij}g_i}\right] = -\frac{E_i}{kT} + \ln\left(\frac{hn}{2\pi Z}\right) \qquad (3)$$

where I_{ij} is the intensity of the transition from level i to level j, λ_{ij} is the wavelength of the transition, A_{ij} is the atomic transition probability, E_i is the energy of the upper level, h is the Planck constant, n is the species density, Z is the electronic partition function, and c is the speed of light in vacuum. Temperature is determined from the slope of the line of right hand side of Equation 3 plotted versus the energy E_i of each upper level in the transition. Since only the slope of

the line is of interest, the values inside the logarithmic terms need only be known relativly to determine temperature. In arcjet plasmas where PLTE conditions usually exist, the lower energy levels are likely to be underpopulated and the resulting transitions from these levels are not in equilibrium with one another. Higher energy levels are more likely to be in collisional, and thus thermal, equilibrium with the electrons of the plasma.[28,31]

Since different energy modes are available within the plasma, several distinct and nonequilibrated temperatures can be thought to exist. Due to sufficient molecular recombination or the lack of dissociation, polyatomic species will exist in the cooler plasma regions of an arcjet nozzle. Two modes of energy deposition, the vibrational and rotational oscillatory modes, can be found for polyatomic species through the use of emission spectroscopy. For this work, the vibrational and rotational temperatures of NH were determined. The vibrational-rotational transitions used to examine NH represent the second most intense spectral features after the hydrogen Balmer series and are in an easily obtained portion of the spectrum.

Vibrational temperature was determined using the integrated intensity ratio of two vibrational-rotational bands and by employing the assumption of LTE. A Boltzmann type plot would have resulted in a more precise measurement and would have also allowed for a determination of the equilibrium within the different vibrational energy levels. However, NH only presented two vibrational transitions that were of sufficient intensity to measure. The two transitions used to determine the NH vibrational temperature were the Q branch $v''=0 \rightarrow v'=0$ and $v''=1 \rightarrow v'=1$ vibrational transitions of the $A^3\Pi \rightarrow X^3\Sigma^-$ molecular transition. These two transitions have band heads at 336.1 and 337.3 nm, respectively. Required NH spectral constants was taken from Lents.[32] Herzberg states that the vibrational temperature can be calculated from the intensity ratio of two molecular bands

$$T_{vib} = \frac{G_1 - G_2}{k \ln\left[\frac{I_2 \lambda_2^4 f_1}{I_1 \lambda_1^4 f_2}\right]} \qquad (4)$$

where G is the energy of the vibrational level and f is the oscillator strength.[28] This method primarily requires that the spectral bands are non-overlapping so that band intensities can be determined unambiguously.

The determination of NH rotational temperature presented a more complicated scenario. First, rotational spectra are nearly always overlapped with other spectral bands and individual transition lines. And second, the rotational spectra within the vibrational-rotational bands of NH were not fully resolved by the spectrometer and CCD detector; therefore, individual rotational transitions were not distinguishable. It is common practice to analytically model the vibrational- rotational spectra, apply an instrument function, and then determine the rotational temperature of the species by the best match with the experimental spectral data. Previous studies of internal arcjet plasma have utilized N_2 and N_2^+ vibrational-rotational bands that are relatively dense and exhibit strong overlap between the various rotational bands.[27,29] NH exhibits what initially appears as a much more open band structure; however, with the instrument resolution available, the triplet structure of the rotational transitions were not fully resolved. Due to the coupling of the rotational angular momentum to the spin angular momentum of the unpaired electrons of the $^3\Pi$ upper and $^3\Sigma^-$ lower states of NH, each of the rotational levels is caused to split into three sub-levels of slightly different energy. For each energy level, the transitions in the R and P branches will be multiplets of three lines having identical angular momentum about the nuclear axis, but different spins.[13,28] A computer code developed by Welle[30] was used to simulate the spectra of the $v''=0 \rightarrow v'=0$ P branch vibrational-rotational transition. The simulated spectra, consisting of a series of transitions with the appropriate wavelengths, are convolved with a line shape to match that seen through the spectrometer and CCD detector. For measurements at maximum dispersion (2400 grooves/mm), a Lorentzian line shape with a full width half maximum of 4 wave numbers matched the data well. The rotational temperature was found by iterating until the best match was found. It was estimated that this iterative procedure was accurate to within 250 K.

Results

The initial viewing throught the optical access ports showed that diagnostics well suited to the plume were not always effective within the arcjet nozzle. Conditions in the furthest downstream access port (hole 3) of the nozzle were found to be similar to those in the plume, while the most upstream port (hole 1) exhibits ionized species not found in the plume.

Boltzmann plots to determine excitation temperatures were attempted for three different species: H, NI, and NII. The hydrogen Balmer series, which is in the visible and near UV region of the spectra, is easily accessible for spectroscopic analysis. However, the Balmer transitions are extremely sensitive to Stark broadening which presented difficulties, especially in port 1. Upper excited state transitions were found to be too broadened and indistinguishable from the background noise. This broadening was exacerbated by overlapping lines, especially in the upstream access ports. Therefore, the Boltzmann plots of the Balmer series, shown in Figure 17, required the use of a moderate dispersion grating (1200 grooves/mm) so that the entire line shape could be collected on the CCD detector. Note that the lower transitions are underpopulated and consequently were not used for determining the best fit slope. Boltzmann plots of the second and third ports were readily obtained and the excitation temperatures were found to be 16,600 and 12,500 K, respectively. Port 1 did not yield a satisfactory number of

clear Balmer transitions for a Boltzmann plot to be generated. In addition to extreme broadening, a number of overlapping lines, primarily from ionized nitrogen, cluttered the signal making line strength determinations impossible. Note that when the two Boltzmann plots are compared, the underpopulation of the lower energy levels is not as severe for hole 2. This implies that the plasma at location 2 is more in equilibrium than is the plasma at location 3. Higher electron density within the nozzle at points further upstream allows for higher electron collisional rates and PLTE is valid at lower energy levels.[33]

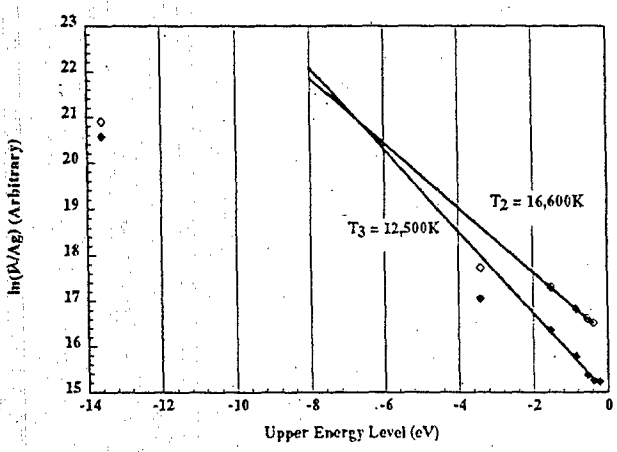

Figure 17: Boltzman Plot of Hydrogen Balmer Series.
(Temperatures are taken at holes #2 and #3)

Figure 18, which shows the Boltzmann plots generated for ionized nitrogen (NII), gives the excitation temperatures for port 1 as 22,000. Unlike the hydrogen Balmer series the NII spectra were not significantly broadened. However, the intensity of the NII spectra were seen to rapidly diminish in the downstream direction. While the spectra was sufficiently intense to allow the generation of Boltzmann plots for the first hole, the line strengths of the spectra from holes 2 and 3 were insufficient to produce meaningful results.

Although Tahara et al and Zube and Myers both used atomic nitrogen (NI) spectra to determine excitation temperatures (Tahara et al by use of a Boltzmann plot and Zube and Myers by line intensity ratio), the NI line strengths were found to be too weak in this study to generate Boltzmann plots.[27,29] The reason for this is not fully understood; however, it should be pointed out that neither of Tahara et al nor Zube and Myers used ammonia as a propellant. Tahara et al used 100% nitrogen and Zube and Myers used simulated hydrazine. Therefore, a likely explanation is that there are differences in the propellant chemistry that have significantly removed the nitrogen atoms from the plasma when NH_3 is used as a propellant mixture rather than N_2 directly.

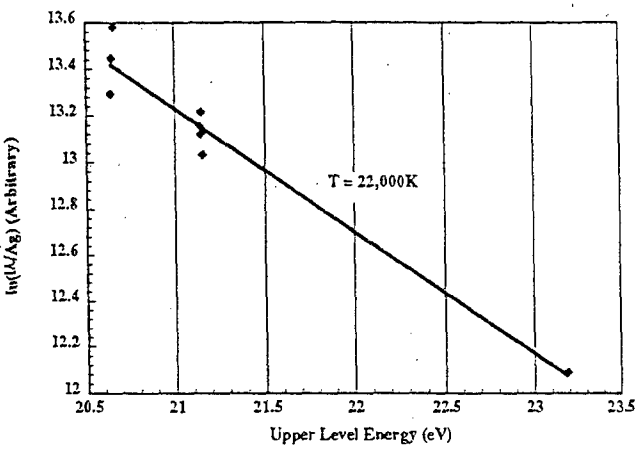

Figure 18: Boltzman Plot of NII.
(Temperature taken at hole #1)

Vibrational and rotational temperatures of NH were determined from the $A^3\Pi \rightarrow X^3\Sigma^-$ transition. The Q branches of the $v'' = 0 \rightarrow v' = 0$ and $v'' = 1 \rightarrow v' = 1$ vibrational transitions were used to determine the vibrational temperature of NH, refer to Figure 19. Vibrational temperatures for ports 1, 2, and 3 were found to be 4300, 4200, and 3750 K, respectively. Rotational temperatures were determined from the P branch of the $v'' = 0 \rightarrow v' = 0$ transition. An example of both the simulated and experimental spectra for hole 3 is shown in Figure 20. Rotational temperatures for ports 1, 2, and 3 were found to be 3750, 3750, and 3500 K, respectively.

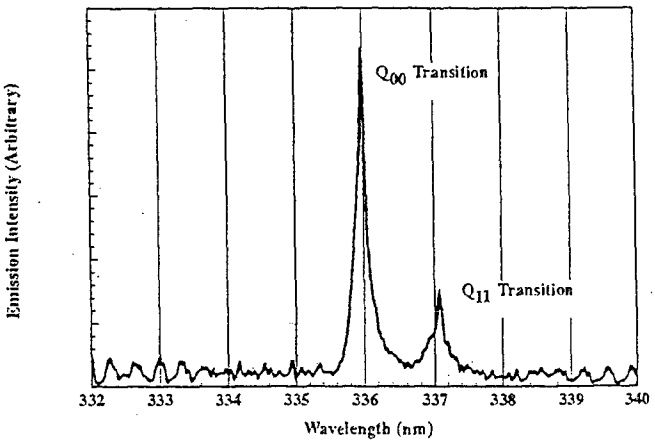

Figure 19: NH Vibrational Transitions

It should be noted that the vibrational temperatures determined here should be treated with extreme caution. Only two transitions lines were available and there is no real way to quantify the effect of nonequilibrium on these measurements. Excluding nonequilibrium effects, it can be assumed that vibrational temperatures are correct to within the uncertainty of the spectral constants (25%); the measurements have an experimental uncertainty of 10%.[27,28] The simulated and experimental matching of the P branch $v'' = 0 \rightarrow v' = 0$ transition exhibited some signs of nonequilibrium.

Nonequilibrium behavior was manifested as a non-Boltzmann population distribution within the rotational energy levels which made temperature determination with the LTE simulation somewhat difficult.

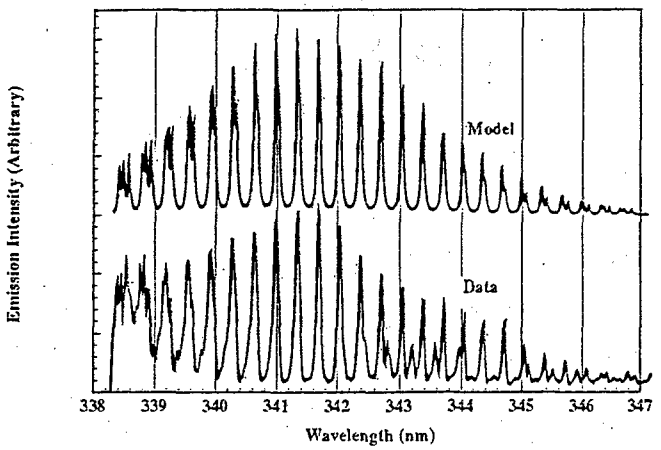

Figure 20: Comparison of Simulated and Experimental NH Spectra

It is important to note that the low molecular temperatures determined for NH as compared to the excitation temperatures of HI and NII are not necessarily a result of nonequilibrium. Rather, the results are primarily an artifact of the gas temperature and density non-uniformity within the arcjet nozzle. NII and to a lesser extent hydrogen are primarily concentrated in the hot inner core flow along the centerline of the nozzle. This region is too hot to support a population of polyatomic particles. Therefore, NH and other polyatomic species are concentrated in the cooler outer portion of the flow along the nozzle inner wall. These two sets of temperatures represent different regions of the line of sight measurement afforded by the optical access ports. Further downstream, the flow becomes frozen and the energy modes, measured by their corresponding temperatures, are isolated and not allowed to equilibrate. The energy remaining in the modes then becomes a function of their relaxation times, which may vary significantly between modes.

Figure 20 illustrates all the measured temperatures for the arcjet during these tests. The HI and NII excitation temperatures can be considered equivalent to the local electron temperature[33] and are observed to fall with the expansion of the flow as expected. Vibrational and rotational temperatures exhibited similar behavior in that they dropped only slightly during the expansion process, but the trend is not as clear as for the electron temperature. Figure 21 shows that the vibrational and rotational modes became frozen early in the expansion and the relaxation times for these modes are longer than the particle residence times in the nozzle. However, the experimental uncertainties are over shadowed by the potential complications of nonequilibrium effects. Vibrational temperature measurements were probably affected by nonequilibrium and caution should be taken in using this data. While the rotational spectra showed some nonequilibrium effects, there is more confidence in the measurements since the experimental spectra compared well to the simulated LTE spectra.

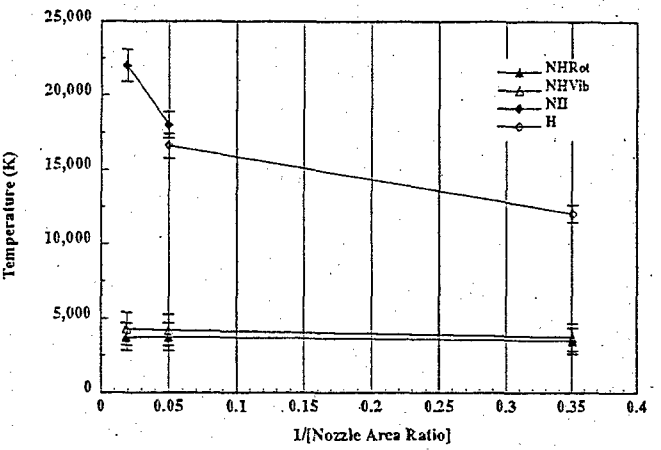

Figure 21: Temperatures within the Arcjet Nozzle

Conclusions

Diagnostics for measuring the species velocity, density and temperature are being developed through a collaborative effort between the Air Force Phillips Laboratory and the University of Southern California. The development of these diagnostics is critical for the improvement of arcjet thruster technology by enhancing the overall understanding of nozzle expansion and as a data base for computational models.

Through the use of Current Modulation Velocimetry, velocity fluctuations are shown to be independent of PPU current ripple. Plume emission appears to be the result of both electron recombination and, to a lesser extent, photon reabsorption from the arc core. At this time it is inconclusive whether the CMV diagnostic is intrusive and further investigation is needed.

Initial Pulsed Electron Beam Fluorescence (PEBF) calibration for helium and nitrogen have been completed. Helium emission was found to be directly proportional to the gas density, making He a propitious gas for developing the PEBF technique. However, nitrogen calibration was found to potentially exhibit non-linear behavior.

Internal emission spectroscopy in a 30kW class arcjet has been demonstrated. NH was found to have vibrational and rotational modes frozen throughout the nozzle expansion. In the upstream region of the nozzle, ionized nitrogen appears to be a strong emitter while in the downstream region, excited H is a good diagnostic species.

Acknowledgments

The CMV work was supported by AFOSR grant F49620-93-1-01213 and AFOSR Task 2308M4. The arcjet and power processing unit were provided by NASA Lewis Research Center. The PEBF work was supported by AFOSR grant F49620-93-1-01213 and URI grant F49620-93-1-0373. We wish to thank Professor E. Phillip Muntz for his assistance in this work. The Emission Spectroscopy work was supported by AFOSR Task 2308M4 and the Air Force Palace Knight Program. We wish to thank Rich Welle for providing us with his NH computational model.

References

1. W. W. Smith et al., "Low Power Hydrazine Arcjet Qualification," IEPC 91-148, 22nd International Electric Propulsion Conference, Viareggio, Italy, October 1991.
2. A. M. Sutton, "Overview of the Air Force ESEX Flight Experiment," IEPC 93-057, 23rd International Electric Propulsion Conference, Seattle, WA, September 1993.
3. C. E. Vaughan and R. J. Cassady, "An Updated Assessment of Electric Propulsion Technology for Near-Earth Space Missions," AIAA 92-3202, 28th Joint Propulsion Conference, Nashville, TN, July 1992.
4. J. E. Pollard, "Arcjet Diagnostics by XUV Absorption Spectroscopy," AIAA 92-2966, 28th Joint Propulsion Conference, Nashville, TN, July 1992.
5. D. H. Manzella and M. A. Cappelli, "Vacuum Ultraviolet Absorption in a Hydrogen Arcjet," AIAA 92-3564, 28th Joint Propulsion Conference, Nashville, TN, July 1992.
6. R. A. Spores, J. A. Pobst, J. H. Schilling, and D. A. Erwin, "Performance Effects of Interaction Between a Low-Power Arcjet and its Power Processing Unit," AIAA 92-3238, 28th Joint Propulsion Conference, Nashville, TN, July 1992.
7. J. A. Pobst, J. H. Schilling, D. A. Erwin, and R. A. Spores, "Time Resolved Measurements of 1 kW Arcjet Plumes using Current Modulation Velocimetry and Triple Langmuir Probes," IEPC 93-128, 23rd International Electric Propulsion Conference, Seattle, WA, September 1993.
8. J. G. Liebeskind, R. K. Hanson, and M. A. Cappelli, "Plume Characteristics of an Arcjet Thruster," AIAA 93-2530, 29th Joint Propulsion Conference, Monterey, CA, June 1993.
9. W. M. Ruyten and D. Keefer, "Laser Fluorescence Velocimetry of an Arcjet Exhaust Plume," IEPC-91-093, 22nd International Electric Propulsion Conference, Viareggio, Italy, October 1991.
10. W. H. Press, B. P. Flannery, S. A. Teukolsky, and W. T. Vetterling, *Numerical Recipes: The Art of Scientific Computing*, 1st ed. (Cambridge Univ. Press, Cambridge, 1986).
11. D. M. Zube and M. Auweter-Kurtz, "Spectroscopic Arcjet Diagnostics under Thermal Equilibrium and Nonequilibrium Conditions," AIAA-93-1792, 29th Joint Propulsion Conference, Monterey, CA, June 1993.
12. E. J. Pencil, J. M. Sankovic, C. J. Sarmiento, J. A. Hamley, "Dependence of Hydrogen Arcjet Operation on Electrode Geometry," AIAA-92-3530, 28th Joint Propulsion Conference, Nashville, TN, July 1992.
13. M. W. Crofton, R. P. Welle, S. W. Janson, and R. B. Cohen, "Rotational and Vibrational Temperatures in the Plume of a 1kW Ammonia Arcjet," AIAA 91-1491, 22nd AIAA Plasmadynamics & Lasers Conference, Honolulu, HI, June 1991.
14. M. A. Cappelli, J. G. Liebeskind, R. K. Hanson, G. W. Butler, D. Q. King, "A Direct Comparison of Hydrogen Arcjet Thruster Properties to Model Predictions," IEPC 93-220, 23rd International Electric Propulsion Conference, Seattle, WA, September 1993.
15. J. H. Schilling, J. A. Pobst, D. A. Erwin, "The Use of Pulsed Electron Beam Fluorescence for Arcjet Plume Diagnostics," IEPC 93-130, 23rd International Electric Propulsion Conference, Seattle, WA, September 1993.
16. D. A. Lichtin, S. W. Janson, J. E. Pollard, D. R. Schulthess, and R. B. Cohen, "Arcjet Plume Characterization Part 1: Mass / Velocity Analyzer Results," AIAA 90-2642, 21st International Electric Propulsion Conference, Orlando, FL, July 1990.
17. E. P. Muntz, "Electron Beam Fluorescence," AGARDograph 132, 1968.
18. J. A. Smith and J. F. Driscoll, "The Electron Beam Fluorescence Technique for Measurements in Hypersonic Turbulent Flows," J. Fluid Mech. 72, 695, 1975.
19. R. M. Wojcik, J. H. Schilling, D. A. Erwin, "Rarefied Flow Diagnostics using Pulsed High-Current Electron Beams," AIAA 90-1515, 1990.
20. R. M. St. John, et al., "Absolute Electron Excitation Cross-Sections of Helium," Phys. Review 134#4A , A888, 1964.
21. M. Mitchner and C. H. Kruger, *Partially Ionized Gases*, 78, Wiley & Sons, 1973.
22. R. M. St. John, et al., "New Process of Excitation Transfer in Helium," Phys. Review 122#6 , 1813, 1961.
23. W. L. Wiese, et al. *Atomic Transition Probabilities, Vol II*, National Bureau of Standards, 1965.
24. K. Frank and J. Christiansen, "The Fundamentals of the Pseudospark and its Applications," IEEE Trans. Plasma Sci. 17, 748, 1989.
25. W. Benker et al., "Generation of Intense Pulse Electron Beams by the Pseudospark Discharge," IEEE Trans. Plasma Sci. 17, 754 (1989).
26. W. Hargus, M. Micci, and R. Spores. "Interior Spectroscopic Investigation of the Propellant Energy Modes in an Arcjet Nozzle," AIAA 94-3302, 30th Joint Propulsion Conference, Indianapolis, IN, June 1994.
27. D. M. Zube, and R. M. Myers, "Nonequilibrium in a Low Power Arcjet Nozzle," AIAA 91-2113, 27th Joint Propulsion Conference, Sacramento, CA, June 1991.
28. G. Herzberg, *Molecular Spectra and Molecular Structure: Volume I - Spectra of Diatomic Molecules*, Krieger Publishing Company, Malabar, FL, 1989.
29. H. Tahara, N. Uda, K. Onoe, and Y. Tsubakishita, "Optical Measurement and Numerical Analysis of Medium Power Arcjet Non-Equilibrium Flowfields," IEPC 93-133, 23rd International Electric Propulsion Conference, Seattle, WA, September 1993.
30. R. P. Welle, Personal Communication, February 1994.
31. R. C. Weast, editor, *Handbook of Chemistry and Physics*, CRC Press, Inc., Boca Raton, FL, 69th edition, 1988.
32. J. M. Lents, "An Evaluation of Molecular Constants and Transition Probabilities for the NH free Radical," Journal of Quantitative Spectroscopy and Radiative Heat Transfer, Vol. 13, p. 297, 1973.
33. H. R. Griem, *Plasma Spectroscopy*, McGraw-Hill Book Company, New York, 1964.